POWER AND ENERGY FUTURE

Open Access
Research Article

Synergistic Stabilization of Heavy Metals during Co-Hydrothermal Carbonization of Sewage Sludge with Lignocellulosic Biomass: Speciation Transformation, Risk Reduction and Sustainability Assessment

Dongyang Wu, Chengxu Sun, and Xuehua Zhang

***Abstract*—With increasing concerns over contamination by heavy metals (HMs) in sewage sludge, treatment technologies integrating detoxification and resource recovery are urgently needed. This study used sewage sludge (SS) and four lignocellulosic biomasses, including pine sawdust (PS), bagasse (BS), sunflower straw (SFS), and water hyacinth (WH), to investigate the migration, transformation, and environmental risks of Cr, Cu, Mn, and Zn during co-hydrothermal carbonization (Co-HTC). Co-HTC reduced the solid-phase concentrations of HMs in hydrochars and promoted their transformation from exchangeable/reducible fractions to oxidizable/residual fractions. The hydrochar derived from SS and BS (H-SS&BS) showed the best stabilization of Cr and Mn, with oxidizable and residual fractions reaching 88.58% and 63.73%, respectively, whereas the hydrochar derived from SS and PS showed superior immobilization of Cu and Zn, with corresponding fractions of 83.30% and 70.93%, respectively. Risk assessment showed that the geoaccumulation index (I_{geo}) values of Cr, Cu, and Zn in H-SS&BS decreased to 0.65, 1.71, and 3.58, respectively. Life cycle assessment (LCA) indicated that BS and SFS systems had lower overall environmental burdens due to improved fuel quality and energy recovery potential. Overall, Co-HTC provides a promising strategy for the simultaneous stabilization of HMs, risk reduction, and resource recovery from sewage sludge.**

***Index Terms*—Lignocellulosic biomass, co-hydrothermal carbonization, heavy metal migration, risk assessment, life cycle assessment.**

ABBREVIATION

HMs	heavy metals
SS	sewage sludge
PS	pine sawdust
BS	bagasse
SFS	sunflower straw
WH	water hyacinth
HTC	hydrothermal carbonization
Co-HTC	co-hydrothermal carbonization
H-SS&BS	hydrochar derived from SS and BS
LCA	life cycle assessment
HHV	higher heating value
CCI	composite combustion index
XRD	X-ray diffraction
RI	risk index
RAC	risk assessment code
ICP-MS	inductively coupled plasma mass spectrometry
FU	functional unit
GWP	global warming potential
LOP	land occupation potential
FETP	fresh-water ecotoxicity potential
FFP	fossil fuel potential
FEP	freshwater eutrophication potential
WCP	water consumption potential
TAP	terrestrial acidification potential
METP	marine ecotoxicity potential
TETP	terrest rial ecotoxicity potential
HTPc	human toxicity potential, cancer
HTPnc	human toxicity potential, non-cancer
SOP	surplus ore potential
XPS	X-ray photoelectron spectroscopy
XAS	X-ray absorption spectroscopy

Manuscript received 30 May, 2026; accepted 7 July, 2026. *(Corresponding author: Xuehua Zhang, e-mail: xuehua.zhang@ualberta.ca)*

D. Wu, C. Sun and X. Zhang are with the Chemical and Materials Engineering Department, University of Alberta, T6G 1H9, Edmonton, Alberta, Canada.

Color versions of one or more of the figures in this paper are available online at https://doi.org/10.26599/PEF.2026.9650014.

Digital Object Identifier 10.26599/PEF.2026.9650014

I. INTRODUCTION

With the acceleration of urbanization and industrialization, the production of municipal sewage sludge has continued to increase. Global municipal wastewater generation is projected to reach 471.2 and 573.8 billion m^3 by 2030

© The author(s) 2026. Published by Tsinghua University Press.
This is an open access article under the Creative Commons Attribution 4.0 International License (http://creativecommons.org/licenses/by/4.0/).

and 2050, respectively [1]. Sewage sludge is typically characterized by high moisture content and complex composition, and is often enriched with various hazardous contaminants, particularly heavy metals (HMs). Among them, Cr, Cu, Mn, and Zn exhibit considerable biotoxicity, and their migration and transformation behaviors are directly associated with ecosystem safety and human health [2].

At present, landfilling, incineration, anaerobic digestion, and thermochemical conversion remain the main routes for sludge disposal and resource recovery [3], [4], [5]. Although these technologies can achieve sludge volume reduction to some extent, it remains challenging to simultaneously realize HM stabilization, secondary pollution control, and energy recovery [6]. For example, landfilling may cause leachate contamination, incineration can generate HM-enriched ash, and anaerobic digestion has limited capacity for HM immobilization. Therefore, developing sludge treatment technologies that integrate HM stabilization and resource recovery is essential for achieving sludge reduction, detoxification, and valorization.

Hydrothermal carbonization (HTC) has been regarded as a promising approach for sludge valorization because it can directly treat high-moisture organic solid wastes and promote organic matter conversion under subcritical water conditions [7], [8], [9]. During HTC, organic matter undergoes hydrolysis, dehydration, decarboxylation, and condensation reactions, which can improve sludge dewaterability and induce the redistribution of HM speciation, thereby reducing ecological risks. However, hydrochars derived from standalone HTC of sewage sludge (SS) generally suffer from high ash content, limited fixed carbon content, and low calorific value, which restrict their potential for energy utilization [10], [11], [12]. Meanwhile, the potential leaching risk of residual HMs in hydrochars remains a concern. Previous studies have shown that introducing lignocellulosic biomass into SS co-hydrothermal carbonization (Co-HTC) systems can improve the carbon content, energy yield, and fuel quality of hydrochars through synergistic interactions among feedstock components [13]. Our previous study further demonstrated that Co-HTC increased the higher heating value (HHV) of hydrochars from 6.45 $MJ \cdot kg^{-1}$ for H-SS to 12.17–14.87 $MJ \cdot kg^{-1}$, with the highest value of 14.87 $MJ \cdot kg^{-1}$ observed for H-SS&PS. The composite combustion index (CCI) also reached 21.78 × 10^{-7} $min^{-2} \cdot °C^{-3}$, which was markedly higher than that of SS at 3.53 × 10^{-7} $min^{-2} \cdot °C^{-3}$ [14].

The environmental risks of HMs in organic solid wastes depend not only on their total concentrations but also on their chemical speciation. Based on the European Community Bureau of Reference (BCR) sequential extraction method, HMs are generally classified into exchangeable (F1), reducible (F2), oxidizable (F3), and residual (F4) fractions [15], [16]. Among these fractions, F1 and F2 are more mobile and are generally regarded as the main risk-associated fractions, whereas F3 and F4 exhibit higher stability and lower bioavailability. Previous studies have indicated that HTC or Co-HTC can promote the transformation of HMs from active fractions to relatively stable fractions, thereby reducing their potential migration risks [17].

In recent years, increasing attention has been paid to the role of lignocellulosic biomass in enhancing HM immobilization during SS treatment. Previous studies have reported that the addition of biomass such as wood chips and rice husk can reduce the concentrations of certain HMs in hydrochars and increase the proportion of the F4 fraction [18], [19]. However, existing studies have mainly focused on the effects of operating parameters, such as reaction temperature, blending ratio, and residence time, on HM stabilization, while the migration and transformation mechanisms of HMs driven by the synergistic interactions between SS and biomass remain insufficiently understood [20]. In particular, the specific contributions of cellulose, hemicellulose, and lignin to HM immobilization during Co-HTC remain unclear. In addition, current safety assessments have mainly focused on the total concentrations, speciation, and ecological risks of HMs in hydrochar products, while the life-cycle environmental burdens associated with biomass acquisition, transportation, and reaction energy consumption have received limited attention [21], [22], [23]. Therefore, it is necessary to integrate life cycle assessment (LCA) to comprehensively evaluate the environmental sustainability of Co-HTC.

In this study, four biomasses with distinct lignocellulosic compositions were co-hydrothermally carbonized with SS under identical conditions to determine whether differences in cellulose, hemicellulose, lignin, and inorganic matter lead to systematic and metal-specific variations in the stabilization of Mn, Cr, Cu, and Zn. The total concentrations and F1-F4 distributions of HMs were determined, while X-ray diffraction (XRD) was used to provide supporting information on mineral-phase evolution and its potential role in HM immobilization. The geoaccumulation index (I_{geo}), potential ecological risk index (RI), and risk assessment code (RAC) were jointly applied to evaluate total contamination, potential ecological risk, and bioavailability. Furthermore, LCA was conducted to quantify the system-level environmental burdens associated with different biomass-assisted Co-HTC pathways. By integrating speciation transformation, ecological risk reduction, and life-cycle sustainability, this study provides a comprehensive basis for biomass selection and sustainable sewage sludge valorization.

II. Materials and Methods

A. Preparation of Sewage Sludge and Biomass Samples

The SS used in this study was collected from a petrochemical wastewater treatment plant in Northeast China and contained relatively high levels of HMs. Four lignocellulosic biomasses, including pine sawdust (PS), bagasse (BS), sunflower straw (SFS), and water hyacinth (WH), were collected from a farm in Northeast China. All feedstocks were washed to remove surface impurities, dried at 105 °C to constant

weight, ground, passed through an 80-mesh sieve, and then sealed for subsequent use. The basic physicochemical properties and lignocellulosic compositions of the feedstocks are shown in Fig. 1.

B. Hydrothermal Carbonization Experiments

In our previous study [14], the effects of reaction temperature, residence time, and blending ratio on the properties of Co-HTC products derived from SS and biomass were systematically investigated. The results showed that hydrochars with relatively high energy yield and improved fuel quality could be obtained at 230 °C, 60 min, and an SS/biomass mass ratio of 1:1. At 230 °C, the hydrothermal reaction severity was sufficient to promote the hydrolysis, dehydration, decarboxylation, and structural reconstruction of organic components, which could also facilitate the migration and speciation transformation of HMs. A residence time of 60 min provided sufficient time for interactions among sludge-derived organic matter, biomass degradation products, mineral phases, and HMs. In addition, the blending ratio of 1:1 ensured adequate interactions between SS and biomass while maintaining an identical total solid input among the different systems. Therefore, these conditions provided a balanced and comparable basis for evaluating the effects of different biomasses on HM migration, transformation, and stabilization.

The experiments were conducted in a BAIKAL-500 mL high-pressure reactor (BAIKAL, China) made of 316L stainless steel. For standalone HTC, 30 g of dry SS or biomass feedstock was mixed with 300 mL of ultrapure water and loaded into the reactor. For Co-HTC, 15 g of dry SS and 15 g of dry biomass were mixed and loaded into the reactor with 300 mL of ultrapure water, maintaining a total solid mass of 30 g and a solid-to-liquid ratio of 1:10. Before reaction, high-purity N_2 (99.99%) was introduced into the reactor with continuous stirring for 15 min to remove residual air. The reactor was then heated to 230 °C and maintained for 60 min. After the reaction, the reactor was naturally cooled to room temperature, and the resulting solid-liquid mixture was separated. The solid products were dried to constant weight in a vacuum oven at 105 °C, ground, and passed through an 80-mesh sieve to obtain HTC or Co-HTC hydrochar samples for subsequent analyses of HM content, speciation, and physicochemical properties.

For clarity, the hydrochars obtained from standalone HTC were denoted as H-SS, H-PS, H-BS, H-SFS, and H-WH, respectively. The hydrochars derived from Co-HTC of SS with different biomasses were denoted as H-SS&PS, H-SS&BS, H-SS&SFS, and H-SS&WH, respectively. The yield, HHV, H/C and O/C atomic ratios, and elemental composition of the HTC and Co-HTC hydrochars are shown in Fig. 2, which were used to support the analysis of biomass-induced changes in hydrochar fuel quality and structural evolution.

The yield and basic properties of hydrochars obtained from HTC and Co-HTC are shown in Fig. 2. Compared with standalone HTC, Co-HTC increased the hydrochar yield, suggesting a potential synergistic interaction between biomass and SS during the hydrothermal reaction. This synergy may promote condensation, polymerization, and solid-phase reconstruction

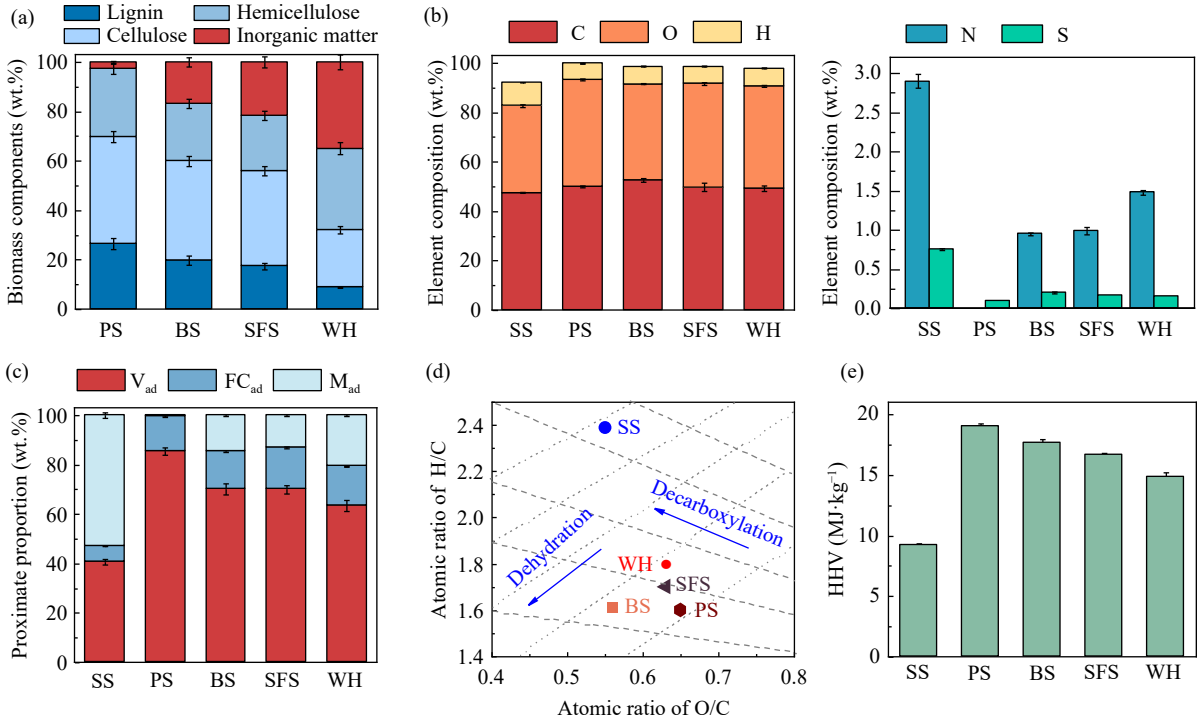


Fig. 1. Basic physicochemical properties of sewage sludge and different biomasses: (a) biomass composition; (b) elemental composition; (c) proximate analysis; (d) H/C and O/C atomic ratios; and (e) higher heating value.

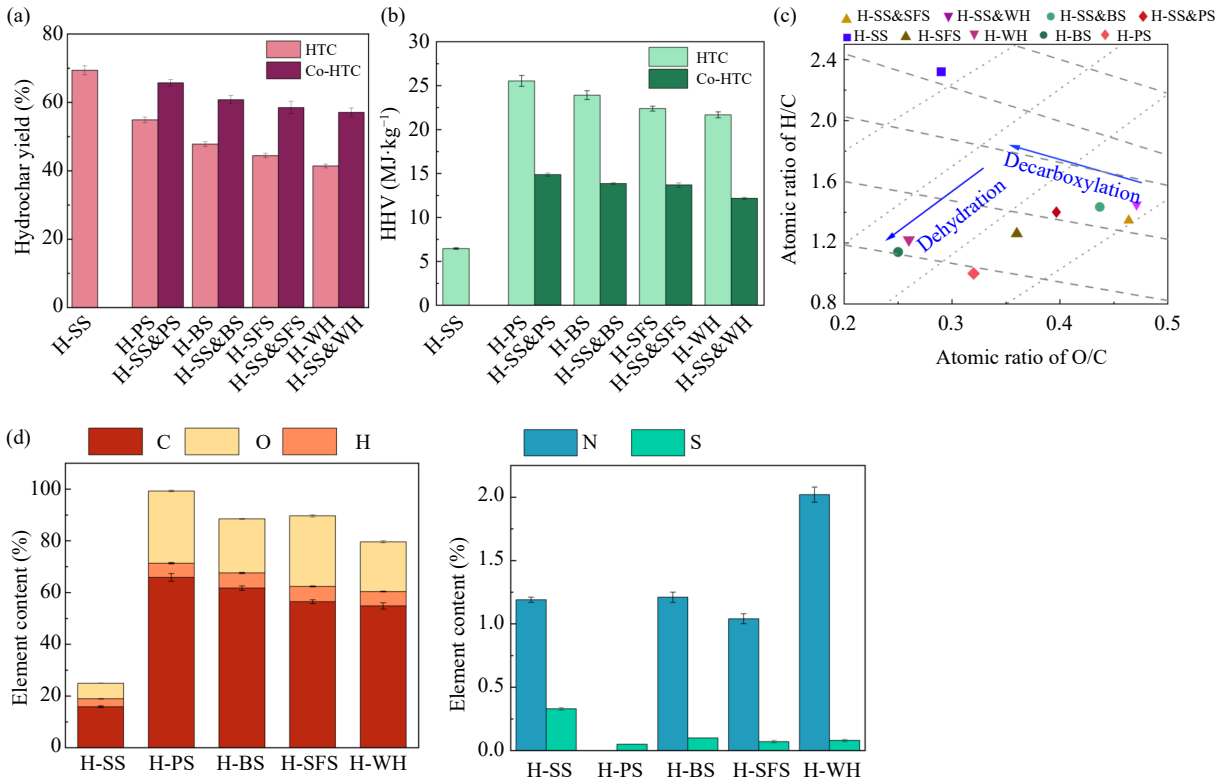


Fig. 2. Yield and basic properties of hydrochars obtained from standalone HTC and Co-HTC: (a) hydrochar yield; (b) higher heating value; (c) H/C and O/C atomic ratios; and (d) elemental composition.

of organic components, thereby inhibiting their further conversion into liquid and gaseous products and retaining more carbon and solid matter in the hydrochar. Such solid-phase retention may provide additional carriers for HM adsorption and complexation, thereby contributing to HM stabilization.

In terms of fuel properties, although the heating value of Co-HTC hydrochars was lower than that of hydrochars derived from standalone biomass HTC, it was markedly higher than that of H-SS obtained from standalone SS HTC. Our previous study showed that Co-HTC increased the HHV of hydrochars from 6.45 MJ·kg^{-1} for H-SS to 12.17–14.87 MJ·kg^{-1}, while increasing the fixed carbon content from 6.16% to 15.01%–21.60%, indicating that biomass addition effectively improved the fuel quality of sludge-derived hydrochars. The decreases in H/C and O/C atomic ratios further indicate that the hydrochars underwent dehydration, decarboxylation, and aromatization, gradually evolving toward carbon-rich and oxygen-depleted structures. This structural evolution suggests enhanced chemical stability and reduced reactivity of hydrochars, which may further contribute to HM immobilization and environmental stability.

C. BCR Sequential Extraction of Heavy Metal Speciation in Samples

When evaluating the environmental and ecological risks of HMs in solid samples, total concentrations alone are insufficient to accurately reflect their potential hazards. Therefore, the BCR sequential extraction method was used to determine the chemical speciation of HMs in this study [15]. This method divides HMs into exchangeable (F1), reducible (F2), oxidizable (F3), and residual (F4) fractions, which correspond to different levels of mobility, bioavailability, and environmental stability.

The extraction procedure was conducted as follows. First, 1.0 g of dry sample was mixed with 40 mL of 0.11 mol·L^{-1} acetic acid solution and shaken at room temperature for 16 h to extract the exchangeable fraction (F1). The residue was then treated with 40 mL of 0.5 mol·L^{-1} hydroxylamine hydrochloride solution, adjusted to pH ≈ 2.0 with nitric acid, and heated at 96 °C for 6 h to extract the reducible fraction (F2). Subsequently, 10 mL of 8.8 mol·L^{-1} hydrogen peroxide was added to the residue, followed by standing at room temperature and water-bath treatment at 85 °C. Then, 50 mL of 1 mol·L^{-1} ammonium acetate solution (pH ≈ 2.0) was added and shaken for 16 h to extract the oxidizable fraction (F3) associated with organic matter or sulfides. Finally, the residue and filter membrane after F3 extraction were transferred into polytetrafluoroethylene digestion vessels, followed by the addition of 8 mL of HNO_3 (65 wt.%), 2 mL of HF (40 wt.%), and 1 mL of H_2O_2 (30 wt.%). Microwave digestion was then performed to obtain the residual fraction (F4).

The extracts obtained from each step were centrifuged, and the concentrations of Mn, Cr, Cu, and Zn in different fractions were determined by inductively coupled plasma mass spec-

trometry (ICP-MS). The above sequential extraction procedure was applied to SS, H-SS, and the four Co-HTC hydrochar samples.

D. Characterization

Following the method reported by Wang et al. [24] for determining total HMs during sludge HTC, with appropriate modifications according to the sample matrices, microwave-assisted acid digestion was performed on raw sludge, raw biomasses, standalone HTC hydrochars, and Co-HTC hydrochars to determine the total concentrations of Mn, Cr, Cu, and Zn. Before analysis, all solid samples were ground to below 200 mesh to improve sample homogeneity and minimize the influence of particle-size differences on digestion efficiency. Digestion was performed using a microwave digestion system (MARS6 Classic, CEM, USA) with a mixed acid solution of HF, HNO_3, and H_2O_2 at a volume ratio of 4:3:1. After digestion, the solution was transferred to an acid evaporation unit (SPB50-24, Tianjin, China) for acid removal and then diluted to 50 mL. The total concentrations of Mn, Cr, Cu, and Zn were determined using ICP-MS (NexION 350, PerkinElmer, USA).

XRD analysis was conducted using an XD-6X diffractometer (Beijing Purkinje General Instrument Co., Ltd., China) to characterize the crystalline structures of raw sludge, raw biomasses, standalone HTC hydrochars, and Co-HTC hydrochars. Before testing, all samples were ground to below 200 mesh and evenly spread in the sample holder to minimize the effects of particle size and uneven sample distribution on diffraction signals. XRD patterns were recorded over a 2θ range of 5°–90°, with a tube voltage of 36 kV, a tube current of 20 mA, and a scanning rate of 10 °·min^{-1}. The crystalline phases and crystallinity changes of the samples were analyzed based on the XRD patterns.

E. Calculation and Assessment Methods

To evaluate changes in HM contamination levels, potential ecological risks, and bioavailability in hydrochars before and after HTC and Co-HTC, the environmental risks of Mn, Cr, Cu, and Zn in SS, H-SS, and the four Co-HTC hydrochars were comprehensively assessed based on total HM concentrations and BCR sequential extraction results.

E.1 Geoaccumulation Index Assessment

I_{geo} was used to evaluate the enrichment of HMs in the samples relative to regional geochemical background values [25]. In this study, the total concentrations of Mn, Cr, Cu, and Zn determined by complete digestion followed by ICP-MS were used to calculate the I_{geo} values of SS, H-SS, and the Co-HTC hydrochars, thereby assessing changes in total HM contamination levels after HTC and Co-HTC. The equation is given as follows

$$I_{geo} = \log_2(\mathrm{Cn}/k\mathrm{Bn}) \tag{1}$$

where Cn represents the mass concentration of a given HM in the sample (mg·kg^{-1}), Bn is the regional geochemical background value of the corresponding element (mg·kg^{-1}), and k is the background correction factor, which was set to 1.5 in this study. Based on the soil elemental background values of Jilin Province, China, the background values of Zn, Cu, Mn, and Cr were set as 52, 17, 600, and 48 mg·kg^{-1}, respectively [26]. The classification criteria for I_{geo} contamination levels are listed in Table 1.

TABLE 1
CLASSIFICATION CRITERIA FOR GEOACCUMULATION INDEX CONTAMINATION LEVELS

I_{geo}	Contamination level	Contamination degree
$I_{geo} \geq 5$	Level 6	Extremely contaminated
$4 \leq I_{geo} < 5$	Level 5	Heavily to extremely contaminated
$3 \leq I_{geo} < 4$	Level 4	Heavily contaminated
$2 \leq I_{geo} < 3$	Level 3	Moderately to heavily contaminated
$1 \leq I_{geo} < 2$	Level 2	Moderately contaminated
$0 \leq I_{geo} < 1$	Level 1	Slightly contaminated
$I_{geo} < 0$	Level 0	Uncontaminated

E.2 Potential Ecological Risk Index Assessment

In this study, the potential ecological risk index method proposed by Hakanson [27] was modified by incorporating the BCR speciation results to evaluate the potential ecological risks associated with differences in HM speciation and toxicity response. Based on the F1–F4 contents of Mn, Cr, Cu, and Zn in SS, H-SS, and the Co-HTC hydrochars, the single-metal contamination factor (C_f), single-metal potential ecological risk factor (E_r), and RI were calculated. Among them, F1+F2+F3 represents the relatively active or potentially mobile fraction, whereas F4 represents the stable residual fraction. The equations are given as follows:

$$C_f = \frac{\mathrm{Ci}}{\mathrm{Cn}} \tag{2}$$

$$E_r = T_r \cdot C_f \tag{3}$$

$$\mathrm{RI} = \sum E_r \tag{4}$$

where Ci is the sum of HM concentrations in the F1+F2+F3 fractions (mg·kg^{-1}); Cn is the HM concentration in the F4 fraction (mg·kg^{-1}); and T_r is the toxicity response coefficient; and RI is the comprehensive potential ecological risk index. According to the Hakanson method and its extended applications, the T_r values of Cu, Zn, Mn, and Cr were set as 5, 1, 1, and 2, respectively. The risk classification criteria are shown in Table 2.

E.3 Risk Assessment Code Method

RAC was used to evaluate the bioavailability and migration risk represented by the exchangeable fraction (F1) of HMs [28]. Based on the BCR sequential extraction results, the proportion of F1 in the total speciation content of Mn, Cr, Cu, and

TABLE 2
CLASSIFICATION CRITERIA FOR SINGLE-METAL POTENTIAL ECOLOGICAL RISK AND COMPREHENSIVE ECOLOGICAL RISK

E_r	Ecological risk level	RI	Ecological risk level
$E_r \le 40$	Low risk	RI ≤ 50	Low risk
$40 < E_r \le 80$	Moderate risk	50 < RI ≤ 100	Moderate risk
$80 < E_r \le 160$	Considerable risk	100 < RI ≤ 150	High risk
$160 < E_r \le 320$	High risk	RI > 150	Very high risk
$E_r > 320$	Very high risk		

Zn in SS, H-SS, and the Co-HTC hydrochars was calculated to assess the effects of different treatments on HM mobility and bioavailability. The equation is given as follows

$$\mathrm{RAC} = \frac{C_{\mathrm{F1}}}{\sum_{i=1}^{n} C_{\mathrm{F1}}} \times 100\% \quad (5)$$

where C_{F1} is the HM content in the F1 fraction (mg·kg^{-1}), and ∑C is the sum of HM contents in all F1–F4 fractions (mg·kg^{-1}). The RAC risk classification criteria are listed in Table 3.

TABLE 3
RISK CLASSIFICATION CRITERIA FOR RISK ASSESSMENT CODE

RAC value	Risk level
0%–1%	No risk
2%–10%	Low risk
11%–30%	Moderate risk
31%–50%	High risk
50%–100%	Very high risk

F. Life Cycle Assessment Method

In this study, LCA was conducted to quantify the environmental impacts of different SS-biomass Co-HTC systems. The LCA model was developed using openLCA software (GreenDelta), with ecoinvent 3.12.1 selected as the background database [29]. The ReCiPe 2016 v1.03 Midpoint (H) method was used for life cycle impact assessment [30]. The functional unit (FU) was defined as the treatment of 1 kg of dry SS, enabling comparison of the environmental impacts of different Co-HTC systems in terms of energy consumption, resource inputs, and pollutant emissions.

The system boundary was defined as cradle-to-gate and covered biomass acquisition, feedstock transportation, the Co-HTC reaction, solid–liquid–gas separation, and product flow allocation, as shown in Fig. 3. The modeling followed the cut-off rule and burden-free approach. Since SS is a waste generated from wastewater treatment, its upstream environmental burden was assumed to have already been allocated to the wastewater treatment system. Therefore, no additional upstream burden was assigned to SS, and the present LCA mainly quantified the incremental environmental burdens associated with biomass acquisition, transportation, water and electricity consumption, and the Co-HTC process. Biomass acquisition and transportation were included as upstream inputs, and differences in feedstock collection and transportation requirements may affect impact categories such as global warming, land occupation, and resource consumption. Therefore, the results should be interpreted as comparative environmental performances under the functional unit, system boundary, inventory assumptions, and zero-burden approach adopted in this study.

The inventory data included feedstock inputs, water and

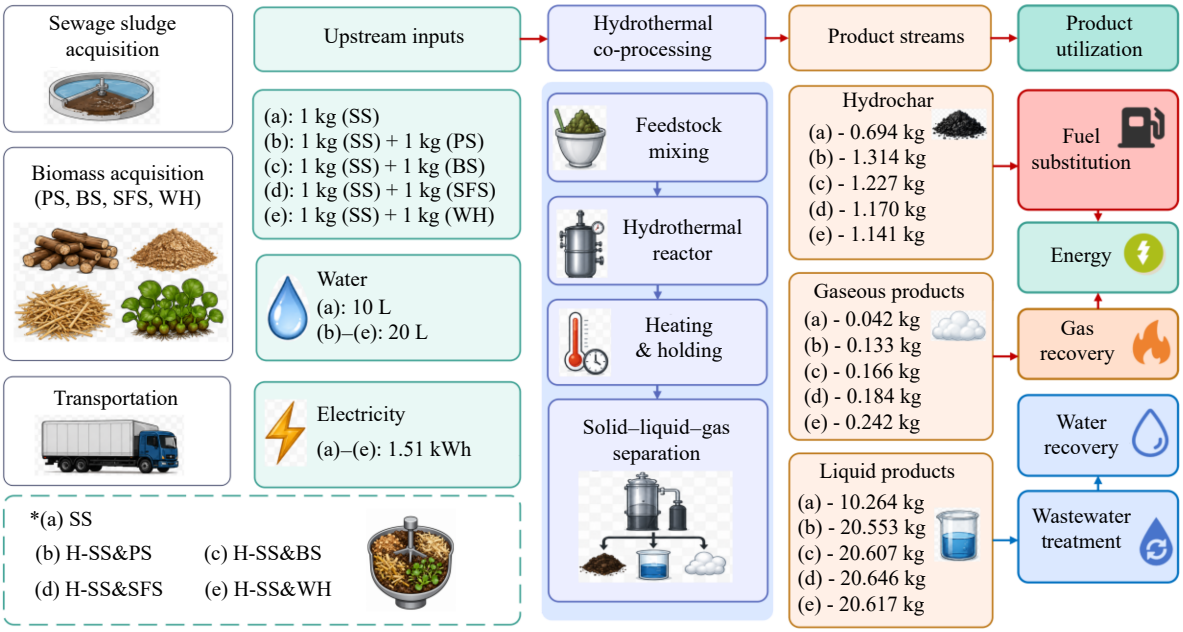


Fig. 3. Life cycle assessment system boundary and material flows of sewage sludge Co-HTC systems with different biomasses.

electricity consumption, product flow allocation, and product utilization pathways. The water input was 10 L for the standalone SS system and 20 L for the SS-biomass Co-HTC systems, while the electricity input was 1.51 kWh for all systems. The outputs of the Co-HTC process mainly included hydrochar, gaseous products, and liquid products. The hydrochar was used for solid fuel substitution, the gaseous products were considered for gas recovery, and the liquid products were directed to water recovery or wastewater treatment. Based on the above material flows and energy inputs, the different treatment pathways were further converted into environmental impact categories, including global warming potential (GWP), land occupation potential (LOP), and freshwater ecotoxicity potential (FETP), to quantitatively compare the overall environmental burdens of different biomass-assisted treatment systems.

III. Results and Discussion

A. Heavy Metal Concentration Analysis

Table 4 lists the total concentrations of Mn, Cr, Cu, and Zn in raw sludge and biomass feedstocks, standalone HTC hydrochars, and Co-HTC hydrochars. The HM concentrations in SS followed the order of Zn > Mn > Cr > Cu. After HTC, the concentrations of Zn, Mn, Cr, and Cu in H-SS increased by 22.48%, 11.76%, 18.47%, and 18.72%, respectively. This increase was mainly attributed to organic matter decomposition and solid mass loss during HTC, which led to the relative enrichment of HMs in the hydrochar. Lang et al. [10] also reported that HMs tend to be enriched in the solid phase after hydrothermal treatment. In addition, organic matter decomposition, mineral precipitation, and metal complexation during HTC can affect the dissolution and solid-phase enrichment behaviors of HMs such as Cu, Cr, and Zn [31].

Compared with H-SS, the HM concentrations in Co-HTC hydrochars generally decreased, indicating that biomass addition helped reduce the solid-phase HM burden in hydrochars. Among the Co-HTC samples, H-SS&BS exhibited the lowest total HM concentration, suggesting that the BS system showed the most pronounced overall reduction effect. This could be partly attributed to the dilution effect caused by the addition of biomass with low HM contents. Moreover, the relatively high cellulose and hemicellulose contents in BS can be readily degraded under hydrothermal conditions to generate small-molecule organic acids and oxygen-containing organics. Functional groups such as hydroxyl, carboxyl, and carbonyl groups may influence HM migration and distribution through complexation or coordination [32]. In addition, Lu et al. [11] reported that the HM contents in cellulose and hemicellulose fractions are generally lower than those in lignin fractions, while biomass with higher lignin content may retain more HMs in Co-HTC hydrochars. Therefore, compared with lignin-rich biomass such as PS, co-treatment of BS with SS was more favorable for reducing the solid-phase HM concentrations in hydrochars.

B. Heavy Metal Speciation Analysis

Total HM concentrations alone are insufficient to accurately evaluate their environmental mobility and ecological risks. Therefore, the BCR sequential extraction method was used to analyze the chemical speciation of HMs (F1–F4) in SS, H-SS, and the four Co-HTC hydrochars. The relative distributions of HMs in the F1–F4 fractions across different samples are presented in Fig. 4, showing the variations in HM speciation after HTC and Co-HTC treatments.

TABLE 4
Total Concentrations of Mn, Cr, Cu, and Zn in Feedstocks, HTC Hydrochars, and Co-HTC Hydrochars

Sample	Mn (mg·kg^{-1})	Cr (mg·kg^{-1})	Cu (mg·kg^{-1})	Zn (mg·kg^{-1})	Total (mg·kg^{-1})
SS	495.145	276.374	193.714	1984.639	2949.872
PS	1.279	0.843	0.425	24.842	27.389
BS	1.328	0.533	0.327	10.438	12.626
SFS	3.225	0.722	0.328	29.322	33.597
WH	25.358	1.372	0.792	73.715	101.237
H-SS	606.451	308.882	229.486	2356.228	3501.047
H-PS	3.313	1.463	0.926	33.774	39.476
H-BS	2.165	1.867	0.433	18.931	23.396
H-SFS	4.339	1.699	0.611	45.668	52.317
H-WH	37.415	2.343	1.338	98.484	139.584
H-SS&PS	340.241	193.522	136.235	1350.654	2020.645
H-SS&BS	310.242	175.613	120.835	1232.014	1838.694
H-SS&SFS	341.231	170.255	132.236	1523.675	2167.387
H-SS&WH	425.322	191.230	163.344	1289.232	2069.233

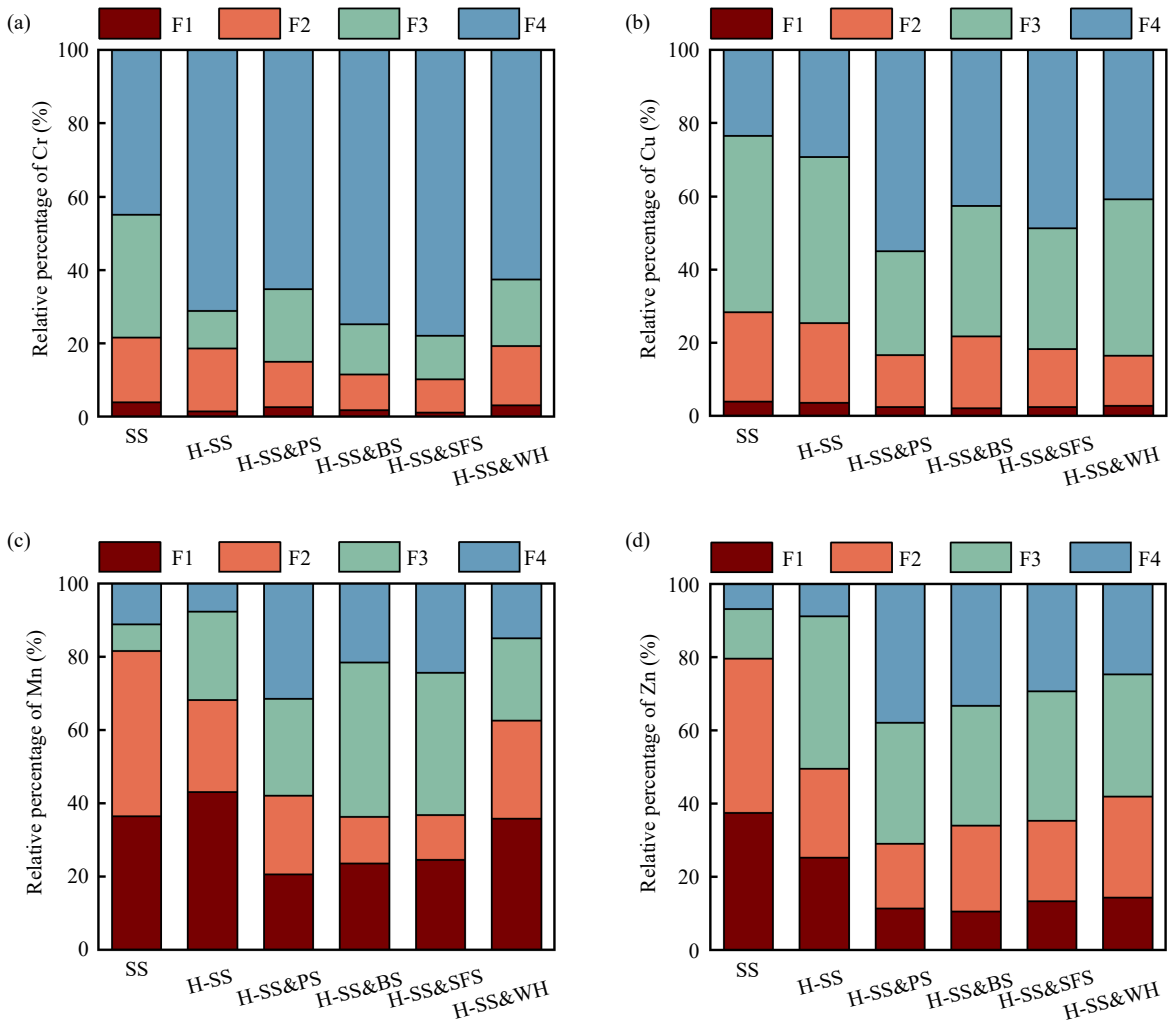


Fig. 4. BCR speciation distribution of Cr, Cu, Mn, and Zn in SS, H-SS, and different Co-HTC hydrochars.

In SS, the speciation distributions of different HMs varied markedly. The F1+F2 proportions of Cr and Cu were relatively low, at 21.54% and 28.29%, respectively, whereas those of Mn and Zn were much higher, reaching 81.59% and 79.57%, respectively. This indicates that Mn and Zn mainly existed in relatively active and mobile fractions in raw sludge, implying higher potential release risks. After Co-HTC, the overall HM speciation shifted from F1/F2 to F3/F4, suggesting that biomass addition promoted the transformation of HMs from active fractions to relatively stable fractions. Among the treatments, H-SS&BS showed a pronounced stabilization effect on Mn and Zn. The F1+F2 proportion of Mn decreased from 81.59% to 36.36%, while its F3+F4 proportion increased from 18.41% to 63.64%. Similarly, the F1+F2 proportion of Zn decreased from 79.57% to 34.04%, whereas its F3+F4 proportion increased from 20.43% to 65.96%. These changes may be associated with organic matter decomposition, functional group reconstruction, and mineral phase transformation during hydrothermal treatment, which could promote the re-binding of active HMs with organic matter, mineral phases, or carbonaceous matrices, thereby reducing their mobility.

The different stabilization behaviors of HMs among the biomass-assisted systems may be related to differences in lignocellulosic composition and hydrothermal degradation characteristics. BS and SFS contained relatively high proportions of cellulose and hemicellulose, which are more susceptible to hydrolysis under hydrothermal conditions. Shi et al. [33] found that the hydrothermal conversion of carbohydrates involved the formation of oxygen-containing intermediates and α-carbonyl compounds, which subsequently participated in condensation and polymerization reactions. Lang et al. [34] reported that the addition of lignocellulosic biomass during Co-HTC altered HM distribution and promoted the transformation of HMs into relatively stable fractions through interactions among organic degradation products, mineral phases, and the hydrochar matrix. Potential hydroxyl, carboxyl, and carbonyl binding sites generated during biomass conversion may also participate in these processes. In contrast, the higher lignin content of PS may favor the stabilization of Cu and Zn. Lignin-derived phenolic hydroxyl, methoxy, and aromatic structures may provide relatively stable adsorption and complexation sites, while the resulting aromatic carbonaceous

matrix may further promote solid-phase association and encapsulation. Therefore, the selective stabilization of different HMs may arise from the combined effects of lignocellulosic degradation products, potential oxygen-containing binding sites, mineral reconstruction, and carbonaceous matrix formation. These proposed pathways should be regarded as plausible interpretations based on the BCR and XRD results together with relevant literature, rather than direct identification of specific metal-binding structures.

However, WH showed irregular effects on HM stabilization, particularly for Cr, for which the F1 proportion increased in H-SS&WH. Previous studies have shown that WH can accumulate HMs such as Cr, Cu, and Zn [35], and its inherent metal burden may affect HM migration and distribution during Co-HTC. During hydrothermal treatment, some HMs accumulated in WH tissues or roots may be re-released and retained in hydrochars in relatively active forms, thereby weakening its dilution and stabilization effects.

It should be noted that the fractions obtained by the BCR sequential extraction method are operationally defined rather than direct representations of the actual molecular or chemical forms of HMs. The measured distributions may be influenced by reagent selectivity, extraction conditions, sample matrix effects, incomplete phase separation, and the redistribution or re-adsorption of released metals during extraction. Therefore, the observed transformation from F1/F2 to F3/F4 should primarily be interpreted as a reduction in potential mobility and bioavailability rather than direct identification of specific metal-binding structures. The proposed stabilization mechanisms should be evaluated together with other characterization results.

C. XRD Analysis of Co-HTC Hydrochars

The XRD patterns of raw sludge, raw biomasses, standalone HTC hydrochars, and Co-HTC hydrochars are presented in Fig. 5, where Fig. 5(a) shows the raw biomasses, Fig. 5(b) shows the standalone HTC hydrochars, and Fig. 5(c) shows the Co-HTC hydrochars. The diffraction peaks in the 2θ range of 13°–18° in Figs. 5(a) and 5(b) were mainly attributed to the ordered crystalline regions of cellulose in lignocellulosic biomass [36], [37]. After HTC, these peaks became markedly weakened and broadened, indicating that the hydrothermal process disrupted the crystalline structure of cellulose and other organic components, thereby reducing the crystallinity of lignocellulosic materials.

As shown in Fig. 5(c), SS exhibited a broad diffraction signal in the 2θ range of 20°–25°, whereas this broad peak weakened after Co-HTC, accompanied by the appearance of several sharper diffraction peaks. This suggests that inorganic mineral phases in sludge underwent reconstruction or recrystallization during the hydrothermal process. Meanwhile, diffraction signals associated with SiO_2 were observed at 2θ = 18°–20° and 21°–23°, indicating that part of the Si in SS may exist as SiO_2 or silicate minerals. These mineral components may provide potential active sites for HM immobilization through surface adsorption, ion exchange, or mineral encapsulation [38].

Combined with the BCR results, Co-HTC promoted the stabilization of HMs to varying degrees. Specifically, H-SS&BS showed better stabilization performance for Mn and Cr, whereas H-SS&PS exhibited stronger immobilization of Cu and Zn. Changes in the intensity and morphology of mineral-phase peaks indicate that mineral dissolution, reconstruction, and re-precipitation may occur during Co-HTC. These processes could provide potential sites for HM adsorption, complexation, co-precipitation, or encapsulation. It should be emphasized that XRD provides indirect information on the evolution of crystalline mineral phases and cannot directly determine HM valence states, local coordination environments, or specific metal-binding structures.Therefore, the pro-

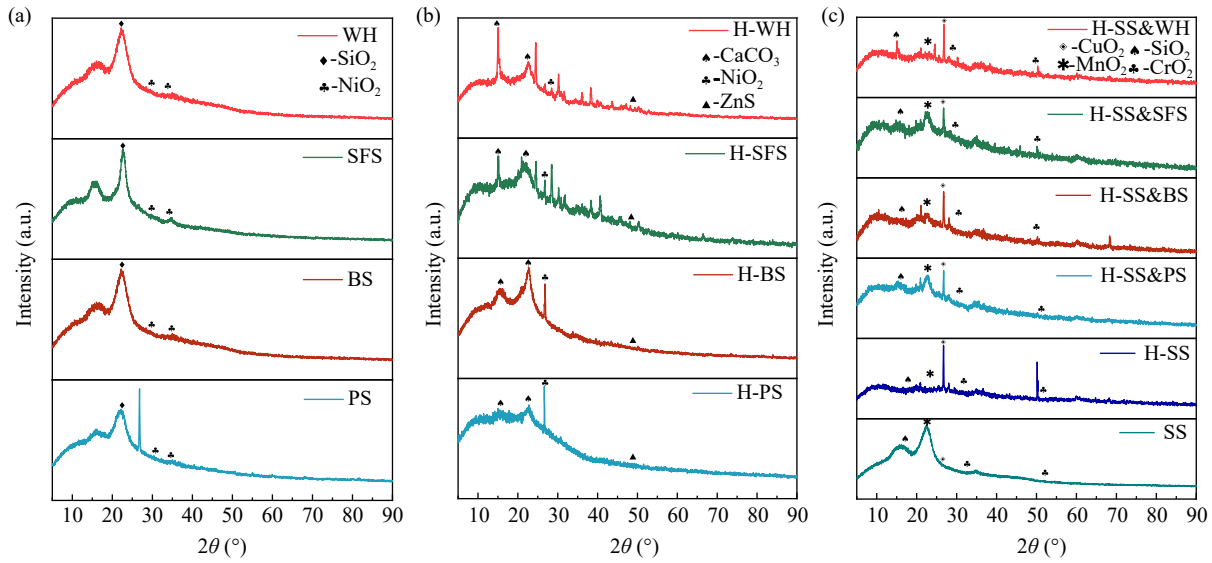


Fig. 5. XRD patterns of raw biomasses, HTC hydrochars, and Co-HTC hydrochars.

posed stabilization pathways should be regarded as plausible mechanistic interpretations supported by the combined BCR and XRD results rather than direct identification of HM binding forms.

D. Comprehensive Assessment of Heavy Metal Environmental Risks

To systematically evaluate the environmental risks of HMs in hydrochars after HTC and Co-HTC, this study conducted a comprehensive assessment from three perspectives: total contamination, potential ecological risk, and bioavailability. Specifically, I_{geo} reflects the enrichment of HMs relative to regional geochemical background values, RI evaluates the potential ecological risk caused by the combined effects of multiple HMs, and RAC indicates the mobility and bioavailability represented by the F1 fraction. This multi-index assessment system provides a more comprehensive evaluation of the actual effectiveness of Co-HTC in reducing HM risks in sewage sludge.

D.1 Geoaccumulation Index Analysis

The I_{geo} values calculated based on total HM concentrations are shown in Fig. 6, with the corresponding contamination levels evaluated according to Table 1. The I_{geo} values of Mn were all below 0, indicating an uncontaminated level. In contrast, the I_{geo} values of Cr, Cu, and Zn in SS were 1.53, 2.55, and 4.39, corresponding to moderate contamination, moderate-to-heavy contamination, and heavy-to-extreme contamination, respectively. After Co-HTC, the I_{geo} values of Cr, Cu, and Zn decreased to varying degrees, suggesting that biomass addition helped reduce the total HM contamination level in hydrochars.

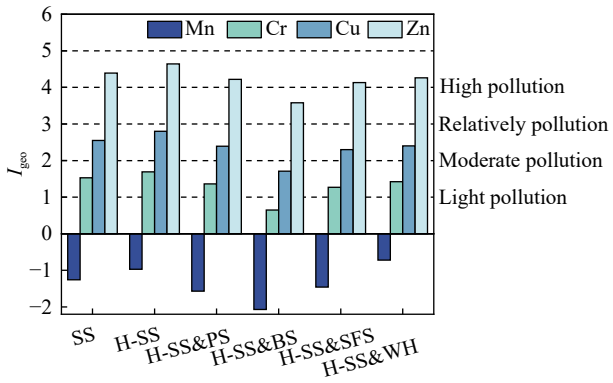


Fig. 6. I_{geo} values of Cr, Cu, Mn, and Zn in SS, H-SS, and different Co-HTC hydrochars.

Among all treated samples, H-SS&BS exhibited the most pronounced contamination reduction. The I_{geo} values of Cr, Cu, and Zn in H-SS&BS decreased to 0.65, 1.71, and 3.58, corresponding to slight contamination, moderate contamination, and heavy contamination, respectively. This result is consistent with the speciation analysis in Section 3.2: H-SS&BS not only reduced the solid-phase HM burden in hydrochars but also promoted the transformation of HMs from active fractions to relatively stable fractions. In particular, the F3+F4 proportions of Cr and Mn reached 88.58% and 63.73%, respectively, indicating that BS showed good stabilization performance for Cr and Mn. This may be related to the high cellulose and hemicellulose contents in BS, whose hydrothermal degradation can generate small-molecule organic acids and oxygen-containing functional groups that participate in HM migration and stabilization through complexation, coordination, or precipitation.

As further shown in Fig. 4, the F1+F2 proportion of Zn in H-SS&BS decreased from 79.57% in SS to 34.04%, while the F3+F4 proportion increased from 20.43% to 65.96%. This speciation transformation indicates that BS addition markedly reduced the bioavailability and mobility of Zn, which was an important reason for the reduction in its environmental risk. Previous studies have also shown that dissolved organic matter and oxygen-containing functional groups generated during hydrothermal treatment can participate in HM complexation and stabilization [39]. Therefore, the H-SS&BS system may promote the transformation of Zn from active fractions to relatively stable fractions through organic complexation, mineral association, and solid-phase encapsulation, thereby reducing its potential ecological risk.

D.2 Potential Ecological Risk Index Analysis

The potential ecological risk assessment results are shown in Fig. 7, with risk levels classified according to the criteria in Table 2. The E_r values of Mn and Cr were both below 40, indicating low ecological risk under the assessment framework used in this study. Specifically, the E_r values of Mn ranged from 0.356 to 0.906, suggesting a low potential ecological risk. Although the E_r values of Cr were higher than those of Mn, they remained below 40. It should be noted that the potential ecological risk index was originally developed for assessing heavy metal contamination in sediments. When applied to matrices such as sludge and hydrochars, the results should be interpreted comprehensively by considering sample

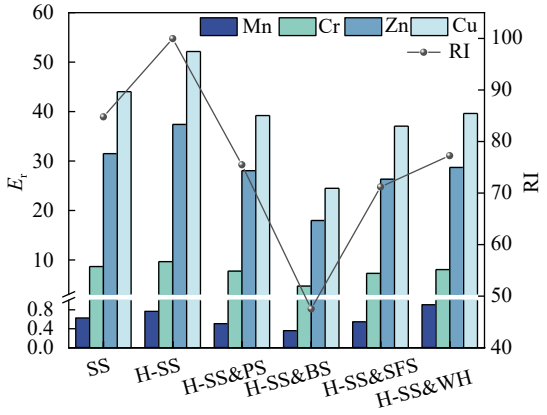


Fig. 7. E_r and RI of Cr, Cu, Mn, and Zn in SS, H-SS, and different Co-HTC hydrochars.

characteristics, background value selection, and speciation distribution [40].

Compared with Mn and Cr, Cu and Zn contributed more to the potential ecological risk. The E_r values of Cu in SS and H-SS were 44.026 and 52.156, respectively, corresponding to a moderate ecological risk level, indicating that standalone HTC did not effectively reduce the potential ecological risk of Cu. After Co-HTC, however, the E_r values of Cu in all Co-HTC hydrochars decreased below 40, reaching the low ecological risk level. A similar decreasing trend was observed for Zn. Among the treatments, H-SS&BS exhibited the most pronounced reduction, with the E_r value of Zn decreasing from 31.5 in SS to 17.9, suggesting that BS addition contributed to reducing the potential ecological risk of Zn.

The RI results showed that H-SS had the highest RI value of 99.975, corresponding to a moderate ecological risk level and approaching the upper limit of this category. This indicates that HM enrichment and the retention of some active fractions in hydrochar after standalone HTC may increase the overall ecological risk. In contrast, the RI value of H-SS&BS was significantly lower than those of the other treated samples, indicating that BS showed better performance in reducing comprehensive ecological risk. As shown in Fig. 4, H-SS&BS markedly promoted the transformation of Mn, Cr, and Zn from active fractions to relatively stable fractions. Specifically, the F1+F2 proportions of Mn and Zn decreased from 81.59% to 36.36% and from 79.57% to 34.04%, respectively, while the F3+F4 proportion of Cr reached 88.58%. These speciation transformations reduced the mobility and bioavailability of HMs, which was a key reason for the decreased comprehensive ecological risk of H-SS&BS.

Overall, the lower RI value of H-SS&BS was mainly attributed to the stabilization of Mn, Cr, and Zn induced by BS. The high cellulose and hemicellulose contents in BS could generate small-molecule organic acids and oxygen-containing functional groups during hydrothermal treatment, thereby promoting the transformation of HMs from F1/F2 fractions to F3/F4 fractions through complexation, coordination, precipitation, or mineral association. Therefore, under the conditions of this study, the H-SS&BS system effectively reduced the comprehensive ecological risk of sludge-derived hydrochars.

D.3 RAC Analysis

According to the RAC results in Fig. 8 and the risk classification criteria in Table 3, the bioavailability risks of different HMs varied markedly. The RAC values of Cr were below 1% in all samples, indicating an extremely low F1 proportion, weak mobility and bioavailability, and a no-risk level. The RAC values of Cu ranged from 4.696% to 9.653%, corresponding to a low-risk level, which was associated with its predominant occurrence in relatively stable fractions such as F3 and F4. In contrast, although Mn showed low total contamination and low potential ecological risk according to the I_{geo} and Er assessments, respectively, its RAC results indicated relatively high risks, with some samples reaching high or very high risk levels. This was mainly because RAC is determined based on the F1 proportion, and Mn exhibited a relatively high F1 proportion in SS and some HTC samples. Previous studies have also emphasized that RAC values are useful for evaluating heavy metal mobilization in solid environmental matrices [41]. Specifically, the F1 proportion of Mn reached 36.51% in SS and even exceeded 50% in H-SS. Therefore, although the overall environmental burden of Mn was relatively low, it may still present certain short-term bioavailability and migration risks.

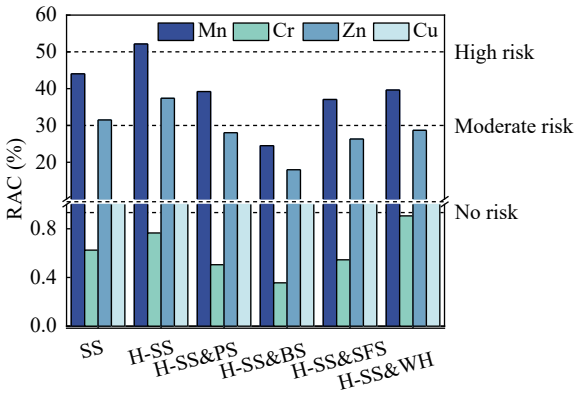


Fig. 8. RAC of Cr, Cu, Mn, and Zn in SS, H-SS, and different Co-HTC hydrochars.

Zn should also be highlighted in the RAC assessment. Owing to its high concentration in SS and hydrochar samples, changes in the active fractions of Zn directly affected its potential ecological risk. After Co-HTC, the RAC value of Zn decreased from the high-risk range (31% < RAC < 50%) to the moderate-risk range (11% < RAC < 30%), indicating that Co-HTC reduced the exchangeable proportion of Zn and thereby weakened its bioavailability and migration risk.

Overall, The three assessment indices describe different aspects of HM environmental risk. I_{geo} mainly reflects the total enrichment of HMs relative to regional background values and is useful for evaluating the overall contamination level. RI considers both potentially mobile fractions and metal-specific toxicity responses, thereby reflecting potential ecological risk. RAC is based exclusively on the F1 proportion and therefore provides a more direct indication of short-term mobility and bioavailability. However, each method has inherent limitations. I_{geo} may be affected by dilution, solid mass loss, and relative enrichment during HTC, while RAC does not consider total HM concentration or toxicity differences. RI provides a broader risk perspective but remains dependent on the selected speciation-based calculation framework and toxicity coefficients. Therefore, no single index can be regarded as universally optimal for Co-HTC products. The combined use of I_{geo}, RI, and RAC provides a more comprehensive assessment from the perspectives of total contamination, potential ecological risk, and bioavailability.

E. Life-Cycle-Based Comprehensive Environmental Impact Assessment

HM risk assessment and LCA evaluate different but complementary aspects of environmental sustainability. I_{geo}, RI, and RAC are based on the total concentrations and speciation distributions of HMs retained in hydrochars and therefore mainly reflect product-level environmental safety, including contamination, ecological risk, mobility, and bioavailability. In contrast, LCA evaluates system-level environmental burdens associated with biomass acquisition, transportation, energy and material inputs, process emissions, and product utilization [42], [43]. It should be noted that toxicity-related indicators in LCA are calculated from life-cycle inventory emissions and characterization factors, whereas the BCR-based risk indices reflect the potential mobility and bioavailability of HMs in hydrochars. Therefore, the two approaches cannot be directly equated, but their combined application provides a more comprehensive evaluation of both product safety and overall process sustainability. Fig. 9 presents the multi-indicator LCA results of the different Co-HTC systems.

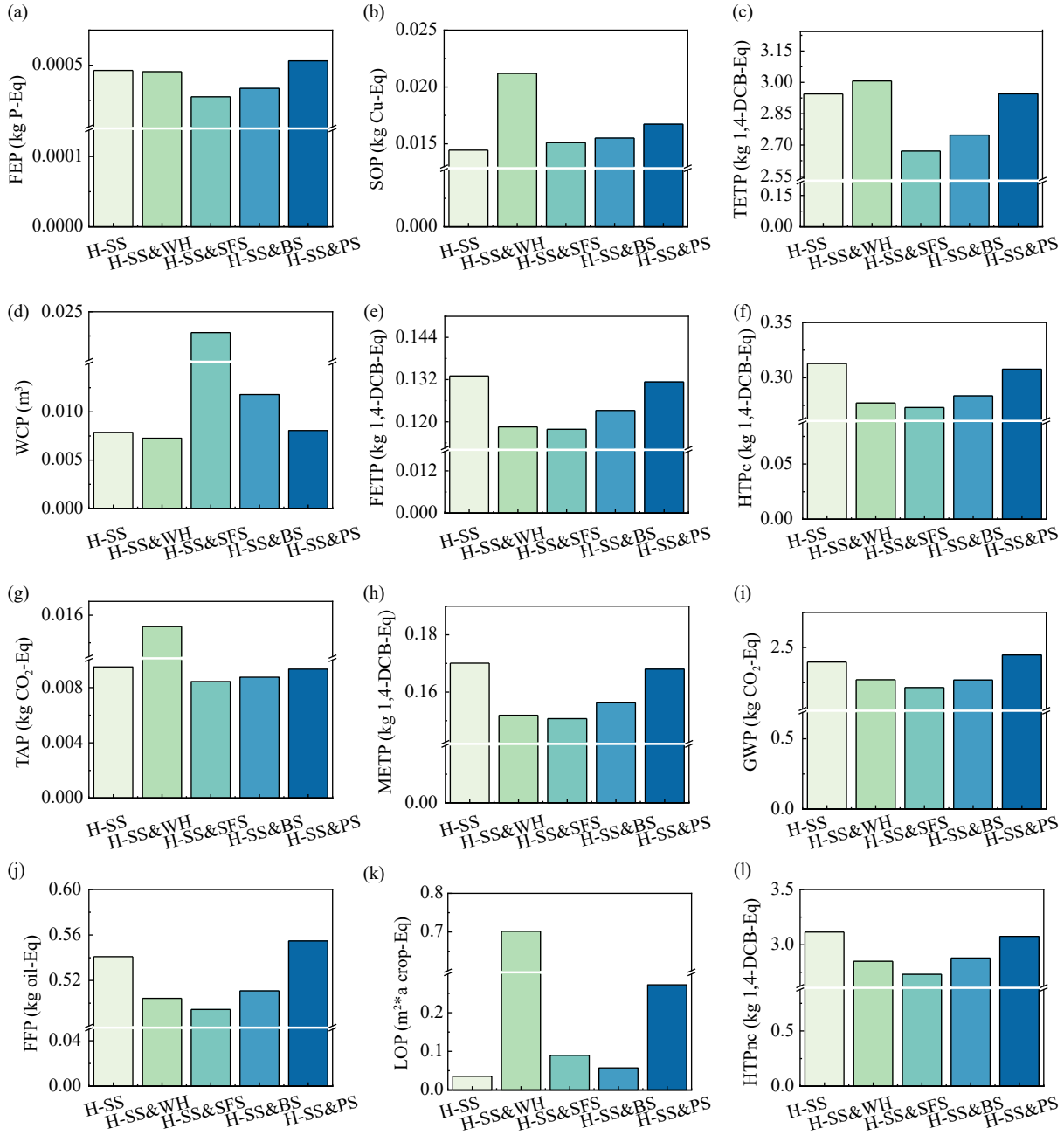


Fig. 9. Life cycle assessment results of different sludge–biomass Co-HTC systems across multiple environmental impact categories: (a) freshwater eutrophication potential (FEP), (b) SOP, (c) TETP, (d) water consumption potential (WCP), (e) FETP, (f) HTPc, (g) terrestrial acidification potential (TAP), (h) marine ecotoxicity potential (METP), (i) GWP, (j) FFP, (k) LOP, and (l) HTPnc.

Overall, the environmental impacts varied markedly among the Co-HTC systems with different biomasses. H-SS&SFS and H-SS&BS showed lower values in most impact categories, especially GWP, fossil fuel potential (FFP), and toxicity-related indicators, suggesting that the addition of SFS and BS helped reduce the overall environmental burden of the Co-HTC systems. Compared with H-SS, the higher heating values of H-SS&SFS and H-SS&BS increased by approximately 47% and 46%, respectively, indicating that their improved fuel quality and energy recovery potential could partially offset the environmental burdens associated with process energy consumption [44]. Specifically, the GWP values of H-SS&SFS and H-SS&BS were 2.2156 and 2.2690 kg of CO_2-Eq, respectively, both lower than that of H-SS (2.3971 kg of CO_2-Eq). Their FETP values were 0.1179 and 0.1232 kg of 1,4-DCB-Eq, and their terrestrial ecotoxicity potential (TETP) values were 2.6712 and 2.7476 kg of 1,4-DCB-Eq, which were also lower than those of H-SS, respectively (0.1330 and 2.9443 kg of 1,4-DCB-Eq). Similar trends were observed for human toxicity indicators. The human toxicity potential, cancer (HTPc) values of H-SS&SFS and H-SS&BS were 0.2731 and 0.2836 kg of 1,4-DCB-Eq, respectively, while their human toxicity potential, non-cancer (HTPnc) values were 2.7319 and 2.8791 kg of 1,4-DCB-Eq, respectively, all lower than those of H-SS. These results indicate that the two systems had lower environmental burdens in ecological and human toxicity-related categories.

In contrast, H-SS&WH showed higher burdens in several impact categories, particularly LOP and surplus ore potential (SOP). The LOP value of H-SS&WH was 0.7018 m^2·a crop-Eq, which was substantially higher than that of H-SS (0.0355 m^2·a crop-Eq) and also much higher than those of H-SS&BS and H-SS&SFS (0.0573 and 0.0899 m^2·a crop-Eq, respectively). As a typical aquatic plant, WH depends strongly on aquatic space during growth and acquisition. Under the LCA inventory and system boundary defined in this study, its feedstock acquisition process was assigned a higher occupation burden, thereby increasing the LOP value. In addition, the SOP value of H-SS&WH was 0.0212 kg Cu-Eq, higher than that of H-SS (0.0144 kg Cu-Eq), indicating that the WH system also imposed a higher mineral resource-related burden. Previous studies have shown that the LCA results of HTC systems are sensitive to system boundaries, functional units, feedstock acquisition routes, and product utilization pathways [45], [46]. Therefore, these results should be interpreted in the context of the modeling assumptions adopted in this study.

Emission-related indicators such as GWP were mainly affected by system energy consumption. During Co-HTC, maintaining the reaction temperature and transporting feedstocks require energy inputs. If the energy is mainly derived from fossil fuels, greenhouse gas emissions will increase. In contrast, SOP mainly reflects the mineral resource burden associated with resource and material inputs within the system. SFS and BS have relatively high organic matter contents and energy recovery potential, which can partially offset process energy consumption by improving hydrochar fuel quality. In contrast, the high moisture content of WH may require additional dewatering or drying energy, thereby increasing its related environmental burdens [47]. For toxicity-related indicators such as FETP, TETP, and HTPc, their variations are associated with pollutant emissions in the life-cycle inventory and the potential migration risks of HMs. Combined with the BCR results in Section 3.2, SFS and BS promoted the transformation of HMs from F1/F2 fractions to F3/F4 fractions, reducing their potential release risks. This may partly explain the decrease in toxicity-related indicators. Nevertheless, LCA toxicity indicators are calculated based on life-cycle inventory emissions and characterization factors, whereas BCR results mainly reflect HM mobility and bioavailability; therefore, the two should not be directly equated.

A reduction in HM risk does not necessarily guarantee an improvement in overall environmental performance. Although enhanced stabilization can reduce the mobility and bioavailability of HMs in hydrochars, additional environmental burdens may arise from biomass acquisition, transportation, drying, electricity consumption, water use, and resource occupation. Consequently, a treatment system with favorable HM immobilization may still exhibit relatively high life-cycle impacts, indicating a potential transfer of environmental burdens from the product stage to upstream or process stages. Under the system boundary and inventory assumptions adopted in this study, the BS and SFS systems showed relatively favorable performance in both HM risk reduction and most LCA impact categories. In contrast, the WH system exhibited higher LOP and SOP values, demonstrating that biomass-specific upstream burdens may offset part of the environmental benefits obtained from HM stabilization. Therefore, LCA is required as a complementary tool to determine whether product-level risk reduction is accompanied by improved system-level environmental sustainability [47], [48].

IV. Conclusions

This study systematically investigated the migration, transformation, speciation evolution, and environmental risk changes of HMs during Co-HTC of SS with four lignocellulosic biomasses, namely PS, WH, SFS, and BS. The results showed that after standalone HTC, the concentrations of Mn, Cr, Cu, and Zn in H-SS increased due to organic matter decomposition and solid-phase enrichment. In contrast, the introduction of biomass generally reduced the solid-phase HM burden in Co-HTC hydrochars. The BCR results indicated that Co-HTC promoted the transformation of HMs from active F1/F2 fractions to relatively stable F3/F4 fractions. H-SS&BS showed better stabilization performance for Cr and Mn, with F3+F4 proportions reaching 88.58% and 63.73%, respectively, whereas H-SS&PS exhibited the best immobilization performance for Cu and Zn, with F3+F4 proportions of 83.30% and 70.93%, respectively. The combined BCR and XRD results

provided indirect evidence that organic matter transformation, mineral phase reconstruction, and carbonaceous matrix formation may jointly contribute to the complexation, adsorption, and immobilization of HMs. Risk assessment results showed that I_{geo}, RI, and RAC generally decreased after Co-HTC, with the I_{geo} values of Cr, Cu, and Zn in H-SS&BS decreasing to 0.65, 1.71, and 3.58, respectively. The LCA results further demonstrated that the environmental performance of Co-HTC was jointly affected by HM stabilization and upstream processes such as biomass acquisition and transportation, with the BS and SFS systems exhibiting relatively better overall environmental benefits.

Nevertheless, the immobilization mechanisms of HMs in this study were mainly inferred from the BCR and XRD results, while direct evidence regarding metal valence states and microscopic binding environments remains insufficient. Future studies should employ X-ray photoelectron spectroscopy (XPS) and X-ray absorption spectroscopy (XAS) to further verify the proposed immobilization pathways. In addition, this study was conducted only under the conditions of 230 °C, 60 min, and an SS/biomass mass ratio of 1:1. Further optimization of reaction parameters, together with continuous operation data and more comprehensive LCA scenarios, is needed to evaluate the engineering application potential of Co-HTC technology.

Declaration of competing interest

The authors declare that they have no known competing financial interests or personal relationships that could have appeared to influence the work reported in this paper.

Acknowledgements

The authors gratefully acknowledge the support provided by National Natural Science Foundation of China (Nos. 52306226 and 52476106), and Jilin Department of Education Science and Technology Research Project, China (No. JJKH20261155KJ).

Use of AI statement

During the preparation of this manuscript, the authors used DeepSeek-V3.2 (DeepSeek, Hangzhou, China), an AI language model, in order to refine the language and improve the readability and grammatical accuracy of the manuscript. The authors have reviewed and edited the content and take full responsibility for the final version of the manuscript.

References

[1] M. Qadir, P. Drechsel, B. J. Cisneros, Y. Kim, A. Pramanik, P. Mehta, and O. Olaniyan, "Global and regional potential of wastewater as a water, nutrient and energy source," *Nat. Resour. Forum*, vol. 44, no. 1, pp. 40–51, Feb. 2020.

[2] B. H. Shi, C. Cheng, Y. Q. Zhang, Z. K. Du, L. S. Zhu, J. Wang, J. H. Wang, and B. Li, "Effects of 3, 6-dichlorocarbazole on microbial ecology and its degradation in soil," *J. Hazard. Mater.*, vol. 424, pp. 127315, Feb. 2022.

[3] A. S. Giwa, N. J. Maurice, H. D. Mendoza, *et al*, "Advances in sewage sludge application and treatment," *Environ. Adv.*, vol. 12, pp. 100389, 2023.

[4] R. Molaey, L. Appels, H. Yesil, A. E. Tugtas, and B. Çalli, "Sustainable heavy metal removal from sewage sludge: A review of bioleaching and other emerging technologies," *Sci. Total Environ.*, vol. 955, pp. 177020, Dec. 2024.

[5] A. Raheem, V. S. Sikarwar, J. He, W. Dastyar, D. D. Dionysiou, W. Wang, and M. Zhao, "Opportunities and challenges in sustainable treatment and resource reuse of sewage sludge: a review," *Chem. Eng. J.*, vol. 337, pp. 616–641, Apr. 2018.

[6] O. S. Djandja, L. X. Yin, Z. C. Wang, and P. G. Duan, "From wastewater treatment to resources recovery through hydrothermal treatments of municipal sewage sludge: a critical review," *Process Saf. Environ. Prot.*, vol. 151, pp. 101–127, Jul. 2021.

[7] D. Kriaučiūnas, T. Žvirblis, K. Kilikevičienė, A. Kilikevičius, J. Matijošius, A. Rimkus, and D. Vainorius, "Impact of simulated biogas compositions (CH_4 and CO_2) on vibration, sound pressure and performance of a spark ignition engine," *Energies*, vol. 14, no. 21, pp. 7037, Oct. 2021.

[8] M. Wilk, A. Magdziarz, K. Jayaraman, M. Szymańska-Chargot, and I. Gökalp, "Hydrothermal carbonization characteristics of sewage sludge and lignocellulosic biomass. A comparative study," *Biomass Bioenergy*, vol. 120, pp. 166–175, Jan. 2019.

[9] T. F. Wang, Y. B. Zhai, Y. Zhu, C. T. Li, and G. M. Zeng, "A review of the hydrothermal carbonization of biomass waste for hydrochar formation: process conditions, fundamentals, and physicochemical properties," *Renew. Sustain. Energy Rev.*, vol. 90, pp. 223–247, Jul. 2018.

[10] D. Cui, X. P. Zhou, S. Wu, H. M. Luk, Q. Y. Lu, J. R. Bai, B. Liu, X. M. Xu, S. Pan, Q. Wang, and X. H. Zhang, "Synergistic mechanism and radicals interaction of the Co-SCWG of cellulose and polystyrene based on ReaxFF-MD and DFT," *J. Energy Inst.*, vol. 125, pp. 102441, Jan. 2026.

[11] X. L. Lu, X. Q. Ma, and X. F. Chen, "Co-hydrothermal carbonization of sewage sludge and lignocellulosic biomass: fuel properties and heavy metal transformation behaviour of hydrochars," *Energy*, vol. 221, pp. 119896, Apr. 2021.

[12] C. Y. Zhang, C. P. Zheng, X. Q. Ma, Y. Zhou, and J. N. Wu, "Co-hydrothermal carbonization of sewage sludge and banana stalk: fuel properties of hydrochar and environmental risks of heavy metals," *J. Environ. Chem. Eng.*, vol. 9, no. 5, pp. 106051, Oct. 2021.

[13] X. Qi, X. Q. Ma, Z. S. Yu, X. L. Lu, S. Liang, and W. Teng, "Addition of water hyacinth and attapulgite during hydrothermal carbonization of sewage sludge: migration behavior of heavy metals and fuel characteristics of hydrochar," *J. Environ. Chem. Eng.*, vol. 10, no. 6, pp. 108857, Dec. 2022.

[14] D. Cui, B. W. Zhang, S. Wu, X. M. Xu, B. Liu, Q. Wang, X. H. Zhang, and J. H. Zhang, "From sewage sludge and lignocellulose to hydrochar by co-hydrothermal carbonization: mechanism and combustion characteristics," *Energy*, vol. 305, pp. 132414, Oct. 2024.

[15] M. Tytła, K. Widziewicz-Rzońca, and Z. Bernaś, "A comparison of conventional and ultrasound-assisted BCR sequential extraction methods for the fractionation of heavy metals in sewage sludge of different characteristics," *Molecules*, vol. 27, no. 15, pp. 4947, Aug. 2022.

[16] J. Wiater and M. Sulewska, "Heavy metal speciation in municipal sewage sludge depending on treatment method," *Desalin. Water Treat.*, vol. 301, pp. 159–172, Jul. 2023.

[17] L. Pola, L. Fernández-García, S. Collado, P. Oulego, and M. Díaz, "Heavy metal solubilisation during the hydrothermal treatment of sludge," *J. Environ. Manage.*, vol. 286, pp. 112120, May 2021.

[18] X. L. Lu, X. Q. Ma, Z. Qin, C. C. Ke, L. M. Chen, and X. F. Chen, "Co-

hydrothermal carbonization of sewage sludge with wood chip: Fuel properties and heavy metal transformation behavior of hydrochars," *Energy Fuels*, vol. 35, no. 19, pp. 15790–15801, Sep. 2021.

[19] W. S. Shi, C. G. Liu, Y. J. Shu, C. P. Feng, Z. F. Lei, and Z. Y. Zhang, "Synergistic effect of rice husk addition on hydrothermal treatment of sewage sludge: fate and environmental risk of heavy metals," *Bioresour. Technol.*, vol. 149, pp. 496–502, Dec. 2013.

[20] L. J. Leng, S. Q. Leng, J. Chen, X. Z. Yuan, J. Li, K. Li, Y. P. Wang, and W. G. Zhou, "The migration and transformation behavior of heavy metals during co-liquefaction of municipal sewage sludge and lignocellulosic biomass," *Bioresour. Technol.*, vol. 259, pp. 156–163, Jul. 2018.

[21] F. Gievers, M. Mainardis, A. Catenacci, A. Loewen, and M. Nelles, "Life cycle assessment of biochar and hydrochar derived from sewage sludge: Material or energy utilization?" *Clean. Environ. Syst.*, vol. 16, pp. 100254, Mar. 2025.

[22] A. Ogunleye, J. Flora, and N. Berge, "Life cycle assessment of hydrothermal carbonization: a review of product valorization pathways," *Agronomy*, vol. 14, no. 2, pp. 243, Jan. 2024.

[23] D. Sinkhonde and T. Bezabih, "On the computational evaluation of carbon dioxide emissions of concrete mixes incorporating waste materials: a strength-based approach," *Clean. Waste Syst.*, vol. 8, pp. 100149, Aug. 2024.

[24] H. Wang, Z. J. Yang, X. Li, and Y. S. Liu, "Distribution and transformation behaviors of heavy metals and phosphorus during hydrothermal carbonization of sewage sludge," *Environ. Sci. Pollut. Res.*, vol. 27, no. 14, pp. 17109–17122, Mar. 2020.

[25] G. Müller, "Index of geoaccumulation in the sediments of the Rhine River, " *GeoJournal*, vol. 2, no. 3, pp. 108–118, 1969.

[26] W. W. Wang, N. Lu, H. Pan, Z. R. Wang, X. Han, Z. C. Zhu, and J. N. Guan, "Heavy metal pollution and its prior pollution source identification in agricultural soil: a case study in the Qianguo irrigation district, northeast China," *Sustainability*, vol. 14, no. 8, pp. 4494, Apr. 2022.

[27] L. Hakanson, "An ecological risk index for aquatic pollution control. a sedimentological approach," *Water Res.*, vol. 14, no. 8, pp. 975–1001, 1980.

[28] G. Perin, L. Craboledda, M. Lucchese, *et al*, "Heavy metal speciation in the sediments of the Northern Adriatic Sea: A new approach for environmental toxicity determination," in *Heavy Metals in the Environment. Vol. 2*, T. D. Lekkas, Eds. Edinburgh: CEP Consultants, 1985, pp. 454–456.

[29] G. Wernet, C. Bauer, B. Steubing, J. Reinhard, E. Moreno-Ruiz, and B. Weidema, "The ecoinvent database version 3 (Part I): Overview and methodology," *Int. J. Life Cycle Assess.*, vol. 21, no. 9, pp. 1218–1230, Apr. 2016.

[30] M. A. J. Huijbregts, Z. J. N. Steinmann, P. M. F. Elshout, G. Stam, F. Verones, M. Vieira, M. Zijp, A. Hollander, and R. Van Zelm, "ReCiPe2016: A harmonised life cycle impact assessment method at midpoint and endpoint level," *Int. J. Life Cycle Assess.*, vol. 22, no. 2, pp. 138–147, Feb. 2017.

[31] X. M. Ke, Z. F. Wu, J. Z. Lin, F. Wang, P. Li, R. C. Xu, M. Yang, L. Han, and D. K. Zhang, "A rapid analytical method for the specific surface area of amorphous SiO_2 based on X-ray diffraction," *J. Non-Cryst. Solids*, vol. 531, pp. 119841, Mar. 2020.

[32] L. M. Madikizela, "Removal of organic pollutants in water using water hyacinth (*Eichhornia crassipes*)," *J. Environ. Manage*, vol. 295, pp. 113153, Oct. 2021.

[33] N. Shi, Q. Y. Liu, X. He, G. Wang, N. Chen, J. Y. Peng, and L. L. Ma, "Molecular structure and formation mechanism of hydrochar from hydrothermal carbonization of carbohydrates," *Energy Fuels*, vol. 33, no. 10, pp. 9904–9915, Aug. 2019.

[34] Q. Q. Lang, Y. C. Guo, Q. F. Zheng, Z. G. Liu, and C. Gai, "Co-hydrothermal carbonization of lignocellulosic biomass and swine manure: Hydrochar properties and heavy metal transformation behavior," *Bioresour. Technol.*, vol. 266, pp. 242–248, Oct. 2018.

[35] H. F. Wen, M. Zhao, J. J. Gao, H. Zhang, and J. Y. Lu, "Stabilization of heavy metals in sewage sludge by co-hydrothermal carbonization with biomass bottom ash," *J. Mater. Cycles Waste Manag.*, vol. 26, no. 3, pp. 1609–1621, Mar. 2024.

[36] A. D. French, "Idealized powder diffraction patterns for cellulose polymorphs," *Cellulose*, vol. 21, no. 2, pp. 885–896, Apr. 2014.

[37] S. L. C. Ferreira, J. B. da Silva, I. F. dos Santos, O. M. C. De Oliveira, V. Cerda, and A. F. S. Queiroz, "Use of pollution indices and ecological risk in the assessment of contamination from chemical elements in soils and sediments-practical aspects," *Trends Environ. Anal. Chem.*, vol. 35, pp. e00169, Sep. 2022.

[38] E. K. He, Y. X. Yang, Z. B. Xu, H. Qiu, F. Yang, W. J. G. M. Peijnenburg, W. H. Zhang, R. L. Qiu, and S. Z. Wang, "Two years of aging influences the distribution and lability of metal(loid)s in a contaminated soil amended with different biochars," *Sci. Total Environ.*, vol. 673, pp. 245–253, Jul. 2019.

[39] Z. X. Yang, X. K. Wan, Y. M. Chen, X. Chen, Z. G. Wang, C. Zhang, V. Kumar, C. Varrone, X. X. Xiao, P. Yu, and W. Huang, "A review of lignin-based adsorbent materials: Synthesis and applications in the remediation of heavy metal/antibiotic-containing wastewater," *J. Environ. Chem. Eng.*, vol. 13, no. 5, pp. 119080, Oct. 2025.

[40] J. B. Liao, X. Y. Cui, H. Feng, and S. K. Yan, "Environmental background values and ecological risk assessment of heavy metals in watershed sediments: a comparison of assessment methods," *Water*, vol. 14, no. 1, pp. 51, Dec. 2021.

[41] G. N. Liang, B. Zhang, M. Lin, S. M. Wu, H. Hou, J. Zhang, G. R. Qian, X. Huang, and J. Z. Zhou, "Evaluation of heavy metal mobilization in creek sediment: Influence of RAC values and ambient environmental factors, " *Sci. Total Environ.*, vol. 607–608, pp. 1339–1347, Dec. 2017.

[42] L. Lombardi, F. Tuci, M. Śliz, K. Czerwińska, S. Fabrizi, and M. Wilk, "Life cycle assessment of the hydrothermal carbonization process applied to the wet fraction mechanically separated from municipal mixed waste," *Waste Manage.*, vol. 166, pp. 181–193, Jul. 2023.

[43] A. Sarrion, E. Medina-Martos, D. Iribarren, E. Diaz, A. F. Mohedano, and J. Dufour, "Life cycle assessment of a novel strategy based on hydrothermal carbonization for nutrient and energy recovery from food waste," *Sci. Total Environ.*, vol. 878, pp. 163104, Jun. 2023.

[44] G. Mannarino, S. Caffaz, R. Gori, and L. Lombardi, "Environmental life cycle assessment of hydrothermal carbonization of sewage sludge and its products valorization pathways," *Waste Biomass Valorization*, vol. 13, no. 9, pp. 3845–3864, Jun. 2022.

[45] M. Owsianiak, M. W. Ryberg, M. Renz, M. Hitzl, and M. Z. Hauschild, "Environmental performance of hydrothermal carbonization of four wet biomass waste streams at industry-relevant scales," *ACS Sustain. Chem. Eng.*, vol. 4, no. 12, pp. 6783–6791, Oct. 2016.

[46] E. Medina-Martos, I. R. Istrate, J. A. Villamil, J. L. Gálvez-Martos, J. Dufour, and Á. F. Mohedano, "Techno-economic and life cycle assessment of an integrated hydrothermal carbonization system for sewage sludge," *J. Clean. Prod.*, vol. 277, pp. 122930, Dec. 2020.

[47] L. Corominas, J. Foley, J. S. Guest, A. Hospido, H. F. Larsen, S. Morera, and A. Shaw, "Life cycle assessment applied to wastewater treatment: state of the art," *Water Res.*, vol. 47, no. 15, pp. 5480–5492, Oct. 2013.

[48] M. Śliz, K. Czerwińska, A. Magdziarz, L. Lombardi, and M. Wilk, "Hydrothermal carbonization of the wet fraction from mixed municipal solid waste: a fuel and structural analysis of hydrochars," *Energies*, vol. 15, no. 18, pp. 6708, Sep. 2022.



Dongyang Wu is currently a Ph.D. student. Supported by the China Scholarship Council, he conducted joint doctoral research at the University of Alberta, Canada. His research interests focus on the efficient thermochemical conversion and valorization of biomass and organic solid waste.



Chengxu Sun is currently a Ph.D. student. Supported by the China Scholarship Council, he conducted joint doctoral research at the University of Alberta, Canada. His research interests include oil shale-assisted water electrolysis for hydrogen production, anodic alternative reactions involving carbonaceous materials, electrochemical interfacial evolution, activation and passivation mechanisms, process modeling of cyclic electrolysis systems, and the hydrothermal conversion and valorization of organic solid waste.



Xuehua Zhang is a Professor at the University of Alberta, a Fellow of the Canadian Academy of Engineering, and the Tier 1 Canada Research Chair in Soft Matter and Interfaces. She earned her Ph.D. in Biomedical Engineering from Shanghai Jiao Tong University, China. In 2014, she was appointed Associate Professor at RMIT University, Australia while concurrently holding a part-time professorship at the University of Twente, Netherlands. She joined the University of Alberta, Canada in 2017 and received the 2025 IUPAC Distinguished Woman in Chemistry or Chemical Engineering Award. Her research employs a multidisciplinary approach combining experimental, theoretical, and numerical methods to advance the understanding in microscopic bubbles and drops in multicomponent systems, the evaporation dynamics of multicomponent droplets, and clean energy solutions and cold plasma technology for advanced water treatment.